Nano Research 2013, 6(12): 906–920
DOI 10.1007/s12274-013-0368-9
Research Article

ISSN 1998-0124
CN 11-5974/O4

Comparative study of gel-based separated arc-discharge, HiPCO, and CoMoCAT carbon nanotubes for macroelectronic applications

Jialu Zhang[§,1], Hui Gui[§,2], Bilu Liu[1], Jia Liu[3], and Chongwu Zhou[1] (✉)

[1] *Department of Electrical Engineering, University of Southern California, Los Angeles, California 90089, USA*
[2] *Department of Material Science, University of Southern California, Los Angeles, California 90089, USA*
[3] *Department of Chemistry, University of Southern California, Los Angeles, California 90089, USA*
[§] *These authors contributed equally to this work.*

Received: 26 June 2013
Revised: 3 September 2013
Accepted: 5 September 2013

KEYWORDS

separated carbon nanotubes, thin-film transistors, gel-based column chromatography, purity of semiconducting nanotubes, diameter-dependence

ABSTRACT

Due to their excellent electrical properties and compatibility with room-temperature deposition/printing processing, high-purity single-walled semiconducting carbon nanotubes hold great potential for macroelectronic applications such as in thin-film transistors and display back-panel electronics. However, the relative advantages and disadvantages of various nanotubes for macroelectronics remains an open issue, despite the great significance. Here in this paper, we report a comparative and systematic study of three kinds of mainstream carbon nanotubes (arc-discharge, HiPCO, CoMoCAT) separated using low-cost gel-based column chromatography for thin-film transistor applications, and high performance transistors—which satisfy the requirements for transistors used in active matrix organic light-emitting diode displays—have been achieved. We observe a trade-off between transistor mobility and on/off ratio depending on the nanotube diameter. While arc-discharge nanotubes with larger diameters lead to high device mobility, HiPCO and CoMoCAT nanotubes with smaller diameters can provide high on/off ratios (> 10^6) for transistors with comparable dimensions. Furthermore, we have also compared gel-based separated nanotubes with nanotubes separated using the density gradient ultracentrifuge (DGU) method, and find that gel-separated nanotubes can offer purity and thin-film transistor performance as good as DGU-separated nanotubes. Our approach can serve as the critical foundation for future carbon nanotube-based thin-film macroelectronics.

1 Introduction

Since first discovered in 1991 [1], carbon nanotubes (CNT) have attracted a lot of attention due to their extraordinary electrical properties such as high intrinsic carrier mobility and current-carrying capacity [2–4].

Address correspondence to chongwuz@usc.edu

TSINGHUA UNIVERSITY PRESS Springer

While significant progress has been made toward making nanoscale transistors based on individual or aligned CNTs for nanoelectronics [5–12], we reported in 2009 that thin-films of separated carbon nanotubes can work as the channel material for thin-film transistors (TFT) used in display back-panel electronics [13]. Other popular TFT channel materials, such as amorphous silicon [14] and organic materials [15–17] suffer from their low carrier mobility, while polycrystalline silicon [18, 19] and metal oxides [20, 21] typically require high-cost and high-temperature processing. Compared with all the materials above, CNT thin-films have the advantages of low-cost room-temperature processing, superb transparency, excellent flexibility, high device performance, and compatibility with printing technologies. During the past four years, inspired by the density-gradient ultracentrifuge (DGU) carbon nanotube separation method developed by Hersam and his coworkers [22, 23], high-performance TFTs using pre-separated semiconducting nanotubes have been fabricated by us and several other groups [13, 24, 25]. In those previous reports, transistors exhibiting high on/off ratio (> 10^5) as well as excellent current drive capability (~1 μA/μm), and their applications such as digital logic circuits [26, 27], transparent electronics [28] and active matrix organic light-emitting diode (AMOLED) displays [29] have been demonstrated.

Recently, several groups [30, 31] have reported a gel-based column chromatographic nanotube separation method, which is very simple and inexpensive. By this method, high-purity semiconducting and even single chirality nanotubes [32, 33] can be separated, and devices fabricated using gel-based separated nanotubes show excellent electrical performance [34]. Due to these merits, gel-based separated semiconducting nanotubes look very promising for TFT applications such as display electronics. In spite of the significant progress reported so far, many interesting issues remain to be studied. For example, among all the mainstream nanotubes, which kind of nanotubes is most suitable for TFT applications? Is the nanotube diameter a key factor affecting the gel-based separated nanotube thin-film transistor (SN-TFT) performance? What are the requirements for TFTs used in AMOELD displays? Are gel-based SN-TFTs good enough for AMOLED display applications? Do gel-based separated nanotubes have electrical properties as good as DGU-based separated nanotubes?

To answer the above-mentioned questions, we report a comparative and systematic study of three kinds of mainstream carbon nanotubes separated using low-cost gel-based column chromatography for macroelectronics applications. Our work includes the following essential components: (1) We carried out gel-based column chromatography for arc-discharge nanotubes (Carbon Solutions, Inc.), HiPCO nanotubes (Unidym, Inc.), and CoMoCAT nanotubes (Sigma-Aldrich, Inc.). High-purity semiconducting nanotubes were achieved; (2) SN-TFTs were fabricated using the three kinds of gel-based separated nanotubes, and key device performance metrics such as on-current density, on/off ratio, sheet resistance and device mobility are directly compared. Based on the detailed analysis, we have revealed a trade-off between transistor mobility and on/off ratio depending on the nanotube diameter, and find that arc discharge nanotubes with larger diameters offer high mobility, while HiPCO and CoMoCAT nanotubes with small diameters can provide high on/off ratio; (3) in addition, we have also compared the electrical properties of gel-based and DGU-based semiconducting nanotubes, and similar electrical performance was observed for both kinds of semiconducting nanotubes. Our gel-based SN-TFT platform shows significant advantages over conventional platforms with respect to cost, scalability, reproducibility, and device performance, and suggests a practical and realistic approach for nanotube-based AMOLED display applications.

2 Results and discussion

To carry out nanotube separation, all three kinds of nanotubes were first dispersed in aqueous solution. Arc-discharge nanotubes were dispersed in water with the assistance of sodium cholate (SC, Sigma-Aldrich, Inc. (99%)) at a concentration of 1 mg/mL, while HiPCO and CoMoCAT nanotubes were dispersed in aqueous solution assisted by 1% sodium dodecyl sulfate (SDS, Sigma-Aldrich (99%)) at 0.3 mg/mL and 1 mg/mL, respectively. Following that, ultra-sonication and centrifugation were applied to these CNT suspensions to remove bundles and impurities. Then, all three kinds of nanotubes went through gel-based separation process. Specifically, Sephacryl medium (GE Healthcare, Inc.) was used to fill the column for succeeding nanotube separation. More details about nanotube dispersion and gel-based column chromatography can be found in the "Methods" section.

After nanotube separation, we characterized the gel-based column chromatographic separated nanotubes. Three kinds of carbon nanotubes, namely arc-discharge nanotubes, HiPCO nanotubes, and CoMoCAT nanotubes were selected and studied in this work. These three kinds of nanotubes have similar defect ratios (Fig. S1 in the Electronic Supplementary Material (ESM)) but very distinct diameter distributions. Arc-discharge nanotubes have diameters which are larger than HiPCO nanotubes and CoMoCAT nanotubes. Due to this diameter difference, different optical and electrical properties were observed for these three kinds of separated nanotubes, which will be discussed later in this article.

Figure 1 shows a comparison of gel-based column chromatographic separated arc-discharge, HiPCO and CoMoCAT nanotubes. The optical absorption spectra before (blue) and after (red) gel-based separation are plotted in Figs. 1(a)–1(c) (a: Arc-discharge nanotubes; b: HiPCO nanotubes; c: CoMoCAT nanotubes). Based on these curves, one can estimate the purity of the separated semiconducting nanotubes, which is 98%, 92%, and 95%, respectively. The purity of separated semiconducting nanotubes is calculated using the optical absorption spectroscopy evaluation [35], which is well accepted by researchers in the carbon nanotube field. This estimation method typically has an error of around a few percent. In this regard, the differences in the purities we obtained with one round of gel chromatography separation are within the error margin of the absorption spectroscopy evaluation. The diameter information can also be extracted, where arc-discharge semiconducting nanotubes exhibit a diameter range of 1.3 nm to 1.7 nm, while HiPCO and CoMoCAT nanotubes show diameters in the range 0.8 nm to 1 nm and ~0.7 nm, respectively. Because of their different diameter distribution, these three kinds of separated nanotubes exhibit different optical properties, which can be seen from the peak positions in the optical absorption spectra, as well as the color of the separated semiconducting nanotube solutions shown in the insets of Figs. 1(a)–1(c) (light brown for arc-discharge semiconducting nanotubes; dark green for HiPCO semiconducting nanotubes; purple for CoMoCAT semiconducting nanotubes). Detailed calculations of the purity and diameter information can be found in ESM Fig. S2.

Other than purity and diameter, nanotube length also plays a crucial role in nanotube thin-film transistor performance. To characterize the length distribution of the three kinds of gel-based separated semiconducting nanotubes, more than one hundred tubes from each kind were imaged and measured by field-emission scanning electron microscopy (FE-SEM), and the histograms are shown in Figs. 1(d)–1(f). From these plots, one can find that arc-discharge nanotubes, HiPCO nanotubes, and CoMoCAT nanotubes show similar average nanotube lengths, which are 540 nm, 617 nm, and 576 nm, respectively. This similarity of nanotube length distribution is due to the fact that a similar nanotube dispersion recipe was employed for all three kinds of nanotubes, which can also be found in the Methods Section. As all these three kinds of separated nanotubes are similar in terms of semiconducting purity and nanotube length, they can be the ideal materials to study the effect of diameter on the electrical performance of SN-TFTs.

To fabricate SN-TFT devices, high density, uniform separated nanotube thin films were deposited on Si/SiO_2 substrates using the solution-based aminosilane-assisted separated nanotube deposition technique reported in our previous publications [13]. FE-SEM was used to inspect the samples after nanotube assembly and the SEM images of the arc-discharge, HiPCO, and CoMoCAT semiconducting nanotubes deposited on Si/SiO_2 substrates are shown in the insets of Figs. 1(d)–1(f), respectively. The nanotube deposition recipes were carefully adjusted so as all three kinds of nanotubes had similar area nanotube density, which was measured to be 32–41 tubes/μm^2 for arc-discharge nanotubes, 27–38 tubes/μm^2 for HiPCO nanotubes, and 26–36 tubes/μm^2 for CoMoCAT nanotubes. After nanotube assembly, the deposited separated nanotube thin films were used for back-gated SN-TFTs fabrication (see Methods). A schematic diagram of the back-gated

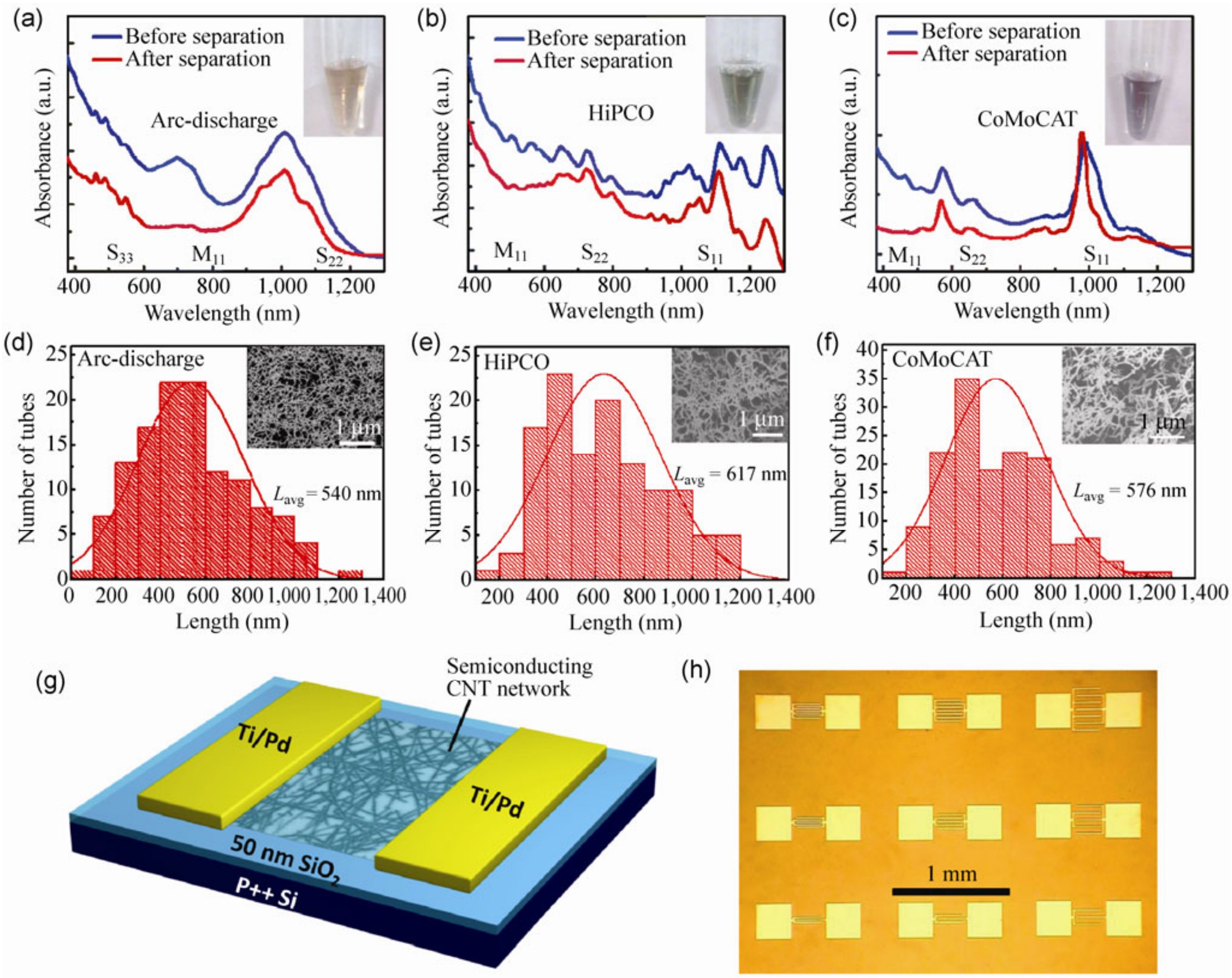

Figure 1 Comparison of gel-based column chromatographic separated nanotubes synthesized by different methods. Optical absorption spectra of arc-discharge nanotubes (a), HiPCO nanotubes (b), and CoMoCAT nanotubes (c) before (blue) and after (red) separation. Inset: Nanotube solutions after separation. Length distribution of the separated semiconducting arc-discharge nanotubes (d), HiPCO nanotubes (e), and CoMoCAT nanotubes (f); the average nanotube length is 540 nm, 617 nm, and 576 nm, respectively. Inset: FE-SEM images of separated semiconducting nanotubes network deposited on Si/SiO_2 substrates with aminopropyltriethoxysilane (APTES) functionalization. (g) Schematic diagram of a back-gated SN-TFT. (h) Optical microscope image of the SN-TFT array fabricated on silicon substrate with 50 nm SiO_2 acting as gate dielectric.

SN-TFTs and the optical microscope image of a fabricated SN-TFT array are shown in Figs. 1(g) and 1(h), respectively.

Electrical performance of gel-separated arc-discharge, HiPCO and CoMoCAT TFTs is compared in Fig. 2. Such SN-TFTs were made with channel width (W) of 200, 400, 800, 1,200, 1,600, and 2,000 μm, and channel length (L) of 4, 10, 20, 50, and 100 μm. Based on these devices, we have carried out systematic measurement and analysis of the electrical performance of the SN-TFTs. Figures 2(a)–2(c) show the normalized transfer characteristics (I_D/W–V_G) of the SN-TFTs using arc-discharge (Fig. 2(a)), HiPCO (Fig. 2(b)) and CoMoCAT (Fig. 2(c)) semiconducting nanotubes with various channel lengths (4, 10, 20, 50, and 100 μm) and fixed channel width (2,000 μm) plotted in logarithm scale. All the curves were measured at V_D = 1 V. From the figures, the following behaviors can be observed: (1) Devices from all nanotube samples show p-type field-effect behavior and very high on/off ratios; (2) as

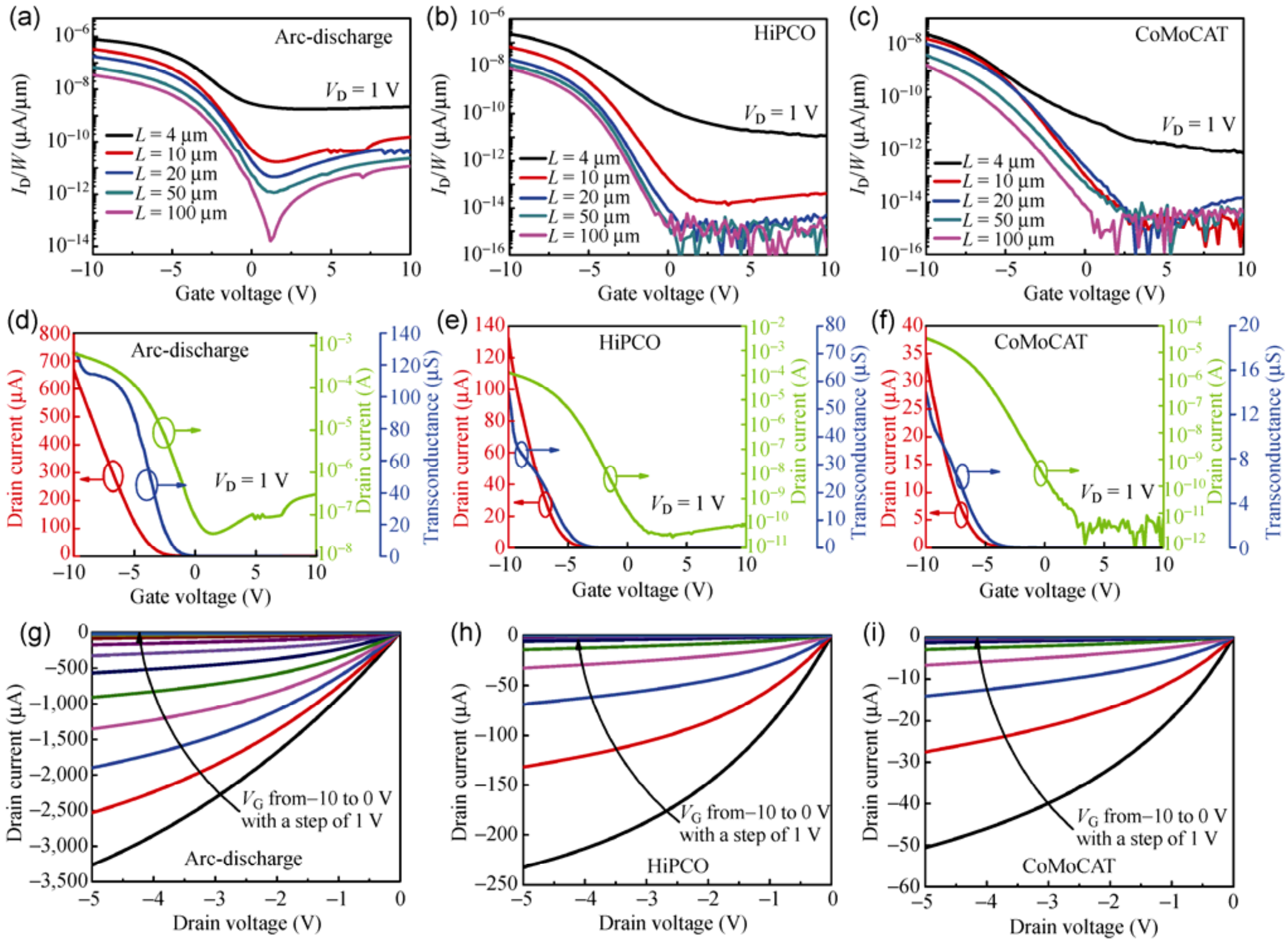

Figure 2 Electrical properties of back-gated SN-TFTs using gel-based separated semiconducting nanotubes synthesized with different methods. Normalized transfer characteristics ($I_D/W - V_G$) of the SN-TFTs using semiconducting arc-discharge nanotubes (a), HiPCO nanotubes (b), and CoMoCAT nanotubes (c) with various channel lengths (4, 10, 20, 50, and 100 μm) and 2,000 μm channel width plotted in logarithm scale. Transfer characteristics (red: Linear scale, green: Log scale) and g_m–V_G characteristics (blue) of a typical SN-TFT (L = 10 μm, W = 2,000 μm) using semiconducting arc-discharge nanotubes (d), HiPCO nanotubes (e), and CoMoCAT nanotubes (f). (g)–(i) Output characteristics (I_D–V_D) of the same devices in (d)–(f).

the device channel length increases, the on/off ratio increases while the on-current decreases. In addition, all three kinds of devices exhibit on/off ratio higher than 10^6 when the channel length is longer than 50 μm; (3) the devices using arc-discharge semiconducting nanotubes with larger diameters exhibit better on-current but lower on/off ratio than HiPCO and CoMoCAT semiconducting nanotubes which have relatively smaller diameters.

Figures 2(d)–2(f) exhibit the transfer characteristics (red: Linear scale, green: Log scale) and g_m–V_G characteristics (blue) of typical SN-TFTs using three kinds semiconducting nanotubes measured at V_D = 1 V. All the devices have a channel length of 10 μm and width of 2,000 μm. Based on these plots, one can find the key device performance metrics of these three devices. For the arc-discharge SN-TFT (Fig. 2(d)), the on-current density (I_{on}/W) at V_D = 1 V and V_G = –10 V is measured to be 0.34 μA/μm, and on/off ratio is 2 × 10^4. The transconductance (g_m) can also be extracted from the maximum slope of the transfer characteristics, which is 113 μS. For the HiPCO SN-TFT (Fig. 2(e)), on-current density is 0.066 μA/μm, on/off ratio is 3.6 × 10^6, and transconductance is 33 μS. For CoMoCAT SN-TFT (Fig. 2(f)), the on-current density, on/off ratio, and transconductance are calculated to be

0.0175 μA/μm, 1.6×10^7, and 10.6 μS, respectively. The corresponding output characteristics (I_D–V_D) of these three SN-TFTs are plotted in Figs. 2(g)–2(i), respectively. Under small V_D biases, the devices exhibit linear behavior, indicating that ohmic contacts are formed between the metal electrodes and the nanotubes. Saturation behavior was observed when more negative V_D was applied, indicating nice field-effect operation.

As mentioned previously, the separated arc-discharge, HiPCO, and CoMoCAT nanotubes have distinctively different diameters, but are similar in length and network density. To get a more comprehensive understanding of the diameter dependent electrical performance behaviour, we have compared the key device performance metrics such as on-current density, channel sheet resistance, on/off ratio, and device mobility for SN-TFTs based on those three kinds of gel-based separated semiconducting nanotubes. Figure 3 summarizes the results after the measurement of 180 SN-TFTs with different semiconducting nanotube diameters, and various channel lengths and channel widths. Figure 3(a) shows the normalized on-current densities (I_{on}/W) of the transistors with various channel lengths measured at $V_D = 1$ V and $V_G = -10$ V, showing that the on-current density is approximately inversely proportional to the channel length for all three kinds of semiconducting nanotubes. The highest on-current density is measured to be 1 μA/μm, which comes from SN-TFTs using separated arc-discharge semiconducting nanotubes with a channel length of 4 μm. Overall, with the same device dimension, SN-TFTs using arc-discharge nanotubes provide about 5 times higher on-current density than the ones using HiPCO nanotubes, and about 17 times higher on-current density than the ones with CoMoCAT nanotubes. This conclusion is also consistent with the data shown in Fig. 2.

To understand the reason for this on-current density difference, we have analysed the contact resistivity and channel sheet resistance of the three different kinds of devices using the transfer length method (TLM). For each transistor, we know that the total device resistance (R_{tot}) is equal to the sum of the contact resistance (R_c) and channel resistance (R_{ch}). As $R_{ch} = R_\square L/W$, where $R_\square$ is the sheet resistance of the separated nanotube film, the total resistance can be described as: $R_{tot} = R_c + R_\square L/W$ or $R_{tot}W = R_cW + R_\square L$. This means that at fixed channel width, the scaled device resistance ($R_{tot}W$) follows a linear relationship with the channel length, while the slope corresponds to the sheet resistance ($R_\square$) and the intercept corresponds to the scaled contact resistance (R_cW). Therefore, using the scaled device resistance data obtained at gate bias of –10 V with different channel length, we can derive the scaled contact resistance and channel sheet resistance of the three different kinds of SN-TFTs, and the results are plotted in Fig. 3(b). From this figure, one can find that the contact resistances for SN-TFTs are negligible compared with channel sheet resistance: The calculated channel sheet resistances for arc-discharge SN-TFTs, HiPCO SN-TFTs, and CoMoCAT SN-TFTs are 0.28 MΩ/□, 1.10 MΩ/□, and 6.52 MΩ/□, respectively. As the sheet resistance is dominated by the tube-to-tube junction resistance [36], we can conclude that large-diameter nanotubes provide smaller junction resistance than small-diameter nanotubes. One contributing factor can be that large-diameter nanotubes have larger tube-to-tube contact area, and therefore smaller junction resistance. Other factors may include how holes transport from one nanotube to another, which needs further study for a thorough understanding. Overall, we find that SN-TFTs using large-diameter nanotubes are superior to the ones using small-diameter nanotubes in terms of channel sheet resistance, which is also the reason why higher on-current density is observed for devices fabricated with larger-diameter nanotubes. As noted before, the differences in the purities of our three kinds of nanotubes are within the error margin of the absorption spectroscopy evaluation. In addition, the metallic nanotube density is way below the percolation threshold to form a conductive path from source to drain, and we therefore believe the above mentioned difference in on-current density mainly comes from the semiconducting nanotube networks.

Besides on-current density, the other important device parameter is current on/off ratio, which is calculated as the current at $V_G = -10$ V divided by the minimum current measured for $V_D = 1$ V; the results are plotted in Fig. 3(c). From this plot, one can find that as the channel length increases, the average on/off

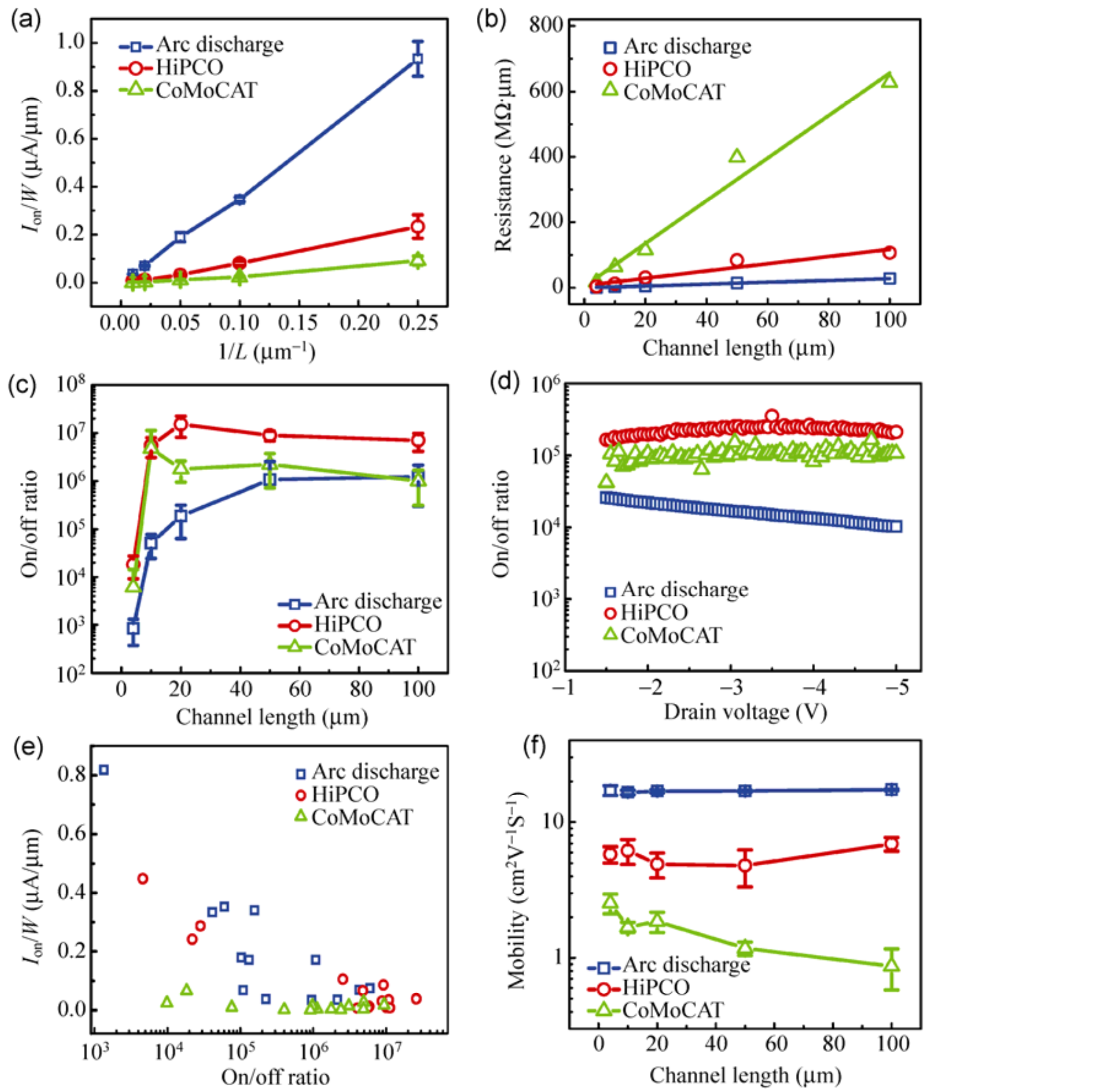

Figure 3 Statistical study and key device performance metrics comparison of SN-TFTs using separated nanotubes with different synthetic methods. (a) Plot of current density (I_{on}/W) versus inverse channel length for TFTs fabricated on separated semiconducting nanotubes synthesized by arc-discharge (blue), HiPCO (red), and CoMoCAT (green) methods. Plot of (b) device resistance and (c) average on/off ratio (I_{on}/I_{off}) versus channel length for the same TFTs characterized in (a). (d) Trade-off between current density (I_{on}/W) and on/off ratio (I_{on}/I_{off}). (e) Plots of on/off ratio (I_{on}/I_{off}) versus drain voltage for devices using three different kinds of semiconducting nanotubes with L = 50 μm and W = 1,200 μm. (f) Relationship between device mobility and channel length for three kinds of SN-TFTs.

ratio of all three kinds of SN-TFTs increases, which is due to the decrease in the probability of percolative transport through metallic nanotubes as the device channel length increases. It is worth noting that for HiPCO and CoMoCAT SN-TFTs, we observe that the average on/off ratio decreases slightly when the channel length is longer than 50 μm. This is because although both the on-current and off-current should decrease when the channel length increases, when the channel length is sufficiently long, the off-current will reach the noise level of the measurement equipment (Agilent 4156 B Semiconducting Parameter Analyzer with an accuracy of 1 pA), and then would not decrease further. Therefore, we observed a slightly decrease of the on/off ratio for long channel devices.

In addition, from Fig. 3(c), we also observe that for the same channel length, the on/off ratios of arc-discharge SN-TFTs is lower than the on/off ratios of HiPCO and CoMoCAT SN-TFTs, which means large-diameter SN-TFTs have higher off-current than small-diameter SN-TFTs. There are two possible sources for the off-current, which are the percolative transport through metallic nanotubes and the thermal excitation of carriers through semiconducting nanotubes [37]. For short channel devices, the former source is believed to be the main reason of the off-current because the channel length is comparable to the length of nanotubes. On the other hand, when the channel length is much longer than nanotube length, based on the 2D stick model [38], the percolation threshold density (N) can be expressed as the following equation

$$N = \frac{1}{\pi}\left(\frac{4.236}{l}\right)^2$$

where l is the average length of the nanotubes. If we take arc-discharge nanotubes as an example (l = 540 nm), N can be calculated to be 20 tubes/μm^2. As only about 2% of the separated arc-discharge nanotubes are metallic, in order to form a metallic pathway for the long channel devices, the total nanotube density needs to reach 1,000 tubes/μm^2, which is much higher than the actual nanotube density we measured (32–41 tubes/μm^2). Therefore, percolative transport through metallic nanotubes is negligible for long channel devices, which suggests that the off-current mainly comes from the thermal excitation of carriers. As we know, the bandgap (E_g) of a nanotube is inversely proportional to the diameter (d) of the nanotube, which can be written as $E_g = 2\gamma_o a_{c\text{–}c}/d$, where γ_o is the C–C tight-binding overlap energy, and $a_{c\text{–}c}$ is the nearest-neighbour C–C distance (0.142 nm). Based on literature, γ_o is around 2.7 eV [3, 4], so that the bandgap ranges for arc-discharge nanotubes, HiPCO nanotubes and CoMoCAT nanotubes are 0.45–0.59 eV, 0.77–0.95 eV, and 1.09 eV, respectively. Thermal excitation can be strongly suppressed for small-diameter separated nanotube TFTs because of their large bandgap. However, for large-diameter nanotubes (arc-discharge nanotubes), due to their small bandgap, non-negligible amounts of thermally excited carriers can be present in the semiconducting nanotubes and flow through the channel to form a non-negligible off-current, which leads to lower on/off ratio than small-diameter nanotube devices (HiPCO and CoMoCAT SN-TFTs). It is worth noting that due to the above-mentioned noise limit of the equipment and the high device resistance for CoMoCAT nanotube thin films, CoMoCAT SN-TFTs exhibit lower on/off ratio than HiPCO SN-TFTs when the channel lengths are long. However, the off-current of CoMoCAT SN-TFTs is actually lower than HiPCO SN-TFTs before it reaches the noise level, as shown in Fig. S3 in the ESM.

The conclusion above is further supported by the results shown in Fig. 3(d), where typical devices using three kinds of nanotubes with the same channel dimension (L = 50 μm, W = 1,200 μm) were characterized. This plot shows that the on/off ratio of the arc-discharge SN-TFTs decreases when the source-to-drain voltage increases, while the on/off ratios for HiPCO and CoMoCAT SN-TFTs remain the same under different drain biases. The decrease in the on/off ratio for arc-discharge SN-TFTs can be attributed to the fact that carriers will gain more energy under a high source-to-drain bias, and therefore, more carriers will be able to transport through the channel due to thermal excitation, which will result in a higher off-current and a lower on/off ratio. In contrast, the wide bandgap of HiPCO and CoMoCAT semiconducting nanotubes can effectively suppress the thermal excitation even under a high source-to-drain voltage, and thus a nearly constant on/off ratio is observed. This phenomenon further proves that instead of percolative transport through metallic nanotubes, thermal excitation of carriers is the main source of the off-current for long channel SN-TFTs. This diameter-dependent on/off ratio behaviour also suggests that small-diameter nanotubes are preferred for applications which need high biases and high on/off ratios.

Interestingly, the data shown in Figs. 3(a) and 3(c) also reveal a trade-off between drive-current and on/off ratio, both of which are key parameters for display applications. On the one hand, larger-diameter nanotubes and shorter channel length can help to achieve higher on-current density due to the small sheet resistance. On the other hand, the narrow bandgap associated with large-diameter nanotubes will give rise to more thermal excitation, and shorter channel length can also increase the possibility of percolative transport through metallic nanotubes, thus leading to higher off-current and lower on/off ratio.

The plot in Fig. 3(e) clearly illustrates this trade-off. One of the most promising applications of carbon nanotube thin-film transistors is AMOLED display electronics, where current drive capability and on/off ratio are the most crucial parameters. Unlike liquid crystal displays (LCD), where a voltage-controlled circuit is applied, a current-controlled circuit is required for AMOLED displays, which means the current flow through the driving transistors will directly go through the OLED pixels, and therefore, determine the output light intensity of the OLED. For this reason, high current drive capability is required for TFTs used in AMOLED displays to create sufficient light intensity within a certain area. For a 40-inch high-definition television (HDTV), in order to reach a brightness of 600 Cd/m^2, a current of about 12 μA needs to be delivered to a pixel with an area of 153 × 460 μm^2 [39], which means that, if a two-transistor control circuit is applied in each pixel, a minimum unit areal current drive of 0.00034 μA/μm^2 needs to be satisfied for the driving transistors in the circuitry. Besides driving current, on/off ratio is another crucial parameter for display electronics. As progressive scanning is used in most display circuits nowadays, each pixel will only be programmed for a very short time during one frame time. In order to have a smooth picture, the switching transistors of each display pixel need to have high enough on/off ratio to keep the light intensity constant. The larger the display, the higher the required on/off ratio, and based on the Ref. [40], on/off ratios needs to reach 10^6 for 256 grayscale 1080P displays. From Fig. 3(e), we can see that for the three kinds of SN-TFTs, if an on/off ratio of 10^6 is required, the highest measured on-current density for arc-discharge SN-TFTs is 0.17 μA/μm, which comes from a device with a channel length of 20 μm, while the highest on-current densities for HiPCO and CoMoCAT SN-TFTs are 0.11 μA/μm (L = 10 μm) and 0.014 μA/μm (L = 10 μm), respectively. In addition, the values of the maximum on-current drive per unit area are 0.0085 μA/μm^2 for arc-discharge SN-TFTs, 0.011 μA/μm^2 for HiPCO SN-TFTs, and 0.0014 μA/μm^2 for CoMoCAT SN-TFTs. One interesting finding is that although having the same channel geometry, arc-discharge SN-TFTs exhibit about 5 times higher on-current density than HiPCO SN-TFTs, and these two kinds of SN-TFTs provide similar maximum on-current drive per unit area for devices with an on/off ratio higher than 10^6. This is due to the trade-off between on-current density and device on/off ratio. Overall, based on our analysis, all three kinds of SN-TFTs meet the basic requirements for transistors used in AMOLED displays.

Besides the on-current density and on/off ratio, we have also characterized device mobility (μ_{device}) for all three kinds of SN-TFTs. Device mobility of the SN-TFTs is extracted following the equation

$$\mu_{\text{device}} = \frac{L}{V_{\text{D}} C_{\text{ox}} W} \cdot \frac{\mathrm{d}I_d}{\mathrm{d}V_g} = \frac{L}{V_{\text{D}} C_{\text{ox}}} \cdot \frac{g_{\text{m}}}{W}$$

where L and W are the device channel length and width, V_{D} = 1 V, and C_{ox} is the gate capacitance per unit area. Here, we use the following equation [41, 42]

$$C_{\text{ox}} = \left\{ C_{\text{Q}}^{-1} + \frac{1}{2\pi\varepsilon_0\varepsilon_{\text{ox}}} \ln\left[\left(\frac{\Lambda_0}{R}\frac{\sinh(2\pi t_{\text{ox}}/\Lambda_0)}{\pi}\right)\right]\right\}^{-1} \Lambda_0^{-1}$$

to calculate the gate capacitance as it considers the electrostatic coupling of nanotubes. Λ_0^{-1} stands for the density of nanotubes and is measured to be around 10 tubes/μm, $C_{\text{Q}} = 4.0 \times 10^{-10}$ F/m is the quantum capacitance of nanotubes [43], and $\varepsilon_0\varepsilon_{\text{ox}} = 3.9 \times 8.85 \times 10^{-14}$ F/cm is the gate dielectric constant. The device mobilities of the three kinds of SN-TFTs are plotted in Fig. 3(f). The arc-discharge SN-TFTs give the highest mobility, which is around 17 cm^2/Vs, whereas HiPCO and CoMoCAT SN-TFTs show lower mobilities around 5 cm^2/Vs and 1 cm^2/Vs, respectively. These data illustrate that large-diameter SN-TFTs provide higher mobility than small-diameter SN-TFTs, which is consistent with the device sheet resistance analysis discussed above. We note that the mobility of around 17 cm^2/Vs we report here for separated arc-discharge tubes is lower than the mobility of around 30 cm^2/Vs we reported previously [26]. One reason is that we used relatively low nanotube density (~32–41 tubes/μm^2) to achieve a high on/off ratio (e.g., > 10^6 for $L \geqslant 50$ μm), while the previous study [26] used 41 tubes/μm^2 to achieve higher mobility at the cost of lower on/off ratio (~10^5). Other factors affecting the mobility include batch-to-batch variation of nanotube quality, variation in nanotube surfactants and length as well as different gate dielectric structures [25].

One important issue we want to point out is that although mobility is the key metric for other thin-film transistor channel materials, it is not the best parameter to evaluate the performance of carbon nanotube TFTs. The reason is that mobility can only directly reflect the current drive capability, but cannot reveal on/off ratio information for the given transistors. This may not be a problem for other TFT channel materials, such as amorphous silicon, polycrystalline silicon, or metal oxides, because all these materials have constant on/off ratio regardless of the channel geometry once their doping level or elemental composition is fixed. However, due to the existence of metallic nanotubes, carbon nanotube TFTs exhibit a trade-off between on-current density and on/off ratio depending on the transistor geometry. Therefore, it is not fair to evaluate the performances of different nanotube TFTs by just comparing the mobility, since this cannot account for the on/off ratio difference between different transistors. One good example is the comparison between arc-discharge and HiPCO SN-TFTs we discussed above. Although arc-discharge SN-TFTs show about three times higher mobility than HiPCO SN-TFTs, these two devices exhibit similar on-current drive when the device on/off ratio is required to be higher than 10^6. For this reason, we think for carbon nanotube TFTs, it is better to compare the maximum current drive capability for a given on/off ratio requirement rather than compare the device mobility alone.

Based on the analysis above, we have found that different separated semiconducting nanotubes exhibit different electrical properties. Table 1 summarizes all the differences we have discussed so far for arc-discharge, HiPCO and CoMoCAT separated nanotubes, including semiconducting nanotube purity, nanotube diameter, electrical bandgap, maximum on-current density for devices with on/off ratio higher than 10^6, device mobility, and channel sheet resistance. Overall, we find that large-diameter nanotubes provide smaller sheet resistance, higher transconductance, and higher device mobility. Hence, large-diameter nanotubes have advantage in applications which require high carrier mobility, such as radio frequency circuits. In contrast, small-diameter nanotubes show higher on/off ratio and smaller off-current, which may be preferred for digital circuit applications, where on/off ratio and

Table 1 Comparison of the properties of arc-discharge, HiPCO, and CoMoCAT separated nanotubes

	Arc-discharge	HiPCO	CoMoCAT
Purity	98%	92%	95%
Diameter (nm)	1.3–1.7	0.8–1.0	~0.7
Energy band (eV)	0.45–0.59	0.77–0.95	~1.09
On-current density when on/off ratio > 10^6 (μA/μm)	0.17	0.11	0.014
Device mobility ($cm^2V^{-1}S^{-1}$)	8.8 ± 0.27	3.0 ± 0.62	0.78 ± 0.067
Sheet resistance (MΩ/□)	0.28	1.10	6.52

power consumption are big concerns. Also, we can conclude that all three kinds of separated nanotubes satisfy the general requirement of AMOLED display applications, which demand a certain current drive and high on/off ratio.

Our ability to fabricate high performance gel-based SN-TFTs enabled us to further explore their application in display electronics. For the proof of concept purpose, an OLED was connected to and controlled by a typical HiPCO SN-TFT device whose transfer characteristic is shown in Fig. S4(a) in the ESM. In order to control the OLED, device on-current and on/off ratio are crucial. Here the device channel length and channel width were selected to be 20 μm and 1,200 μm so that the transistor can provide enough current while the on/off reaches 10^6 and therefore can meet the requirement for controlling the OLED to switch on and off. A standard NPD/Alq_3 OLED (2×2 mm^2) was employed in this study with a multi-layered configuration given as ITO/4-4′-bis[N-(1-naphthyl)-N-phenyl-amino]bi-phenyl (NPD) [40 nm]/tris(8-hydroxyquinoline) aluminium (Alq_3) [40 nm]/LiF [1 nm]/aluminium (Al) [100 nm], and whose transfer characteristics are shown in the Fig. S4(b) in the ESM. The schematic of the OLED control circuit is shown in the inset of Fig. 4(a), where the drain of the driving transistor was connected to an external OLED and a negative voltage (V_{DD}) was applied to the cathode of the OLED. Current flow through OLED (I_{OLED}) can be modified by varying the voltage applied to V_G, as directly revealed in Fig. 5(a) where current versus V_G characteristics are plotted with a fixed V_{DD} of –8 V. From this figure and the inset optical photographs

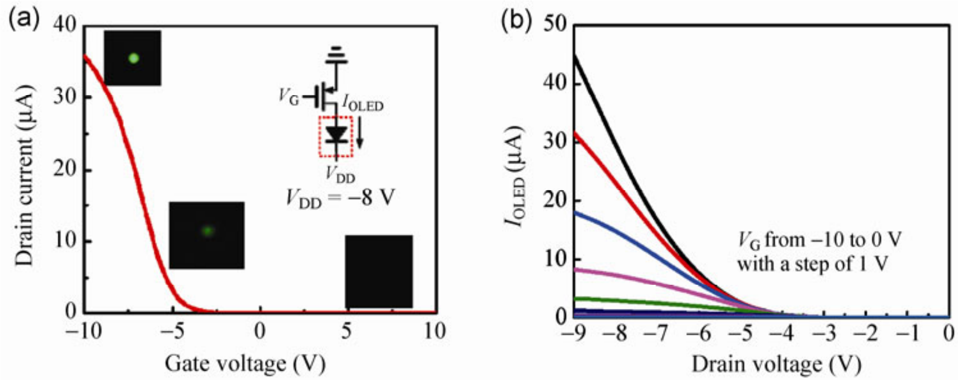

Figure 4 External OLED controlled by HiPCO SN-TFTs. (a) Plot of the current through the OLED (I_{OLED}) versus V_G with V_{DD} = –8 V. The inset optical images show the OLED intensity at certain gate voltages. The inset schematic image is the diagram of the OLED control circuit. (b) I_{OLED} – V_{DD} characteristics of the OLED control circuit. Various curves correspond to various values of V_G from –10 to 0 V in 1 V steps.

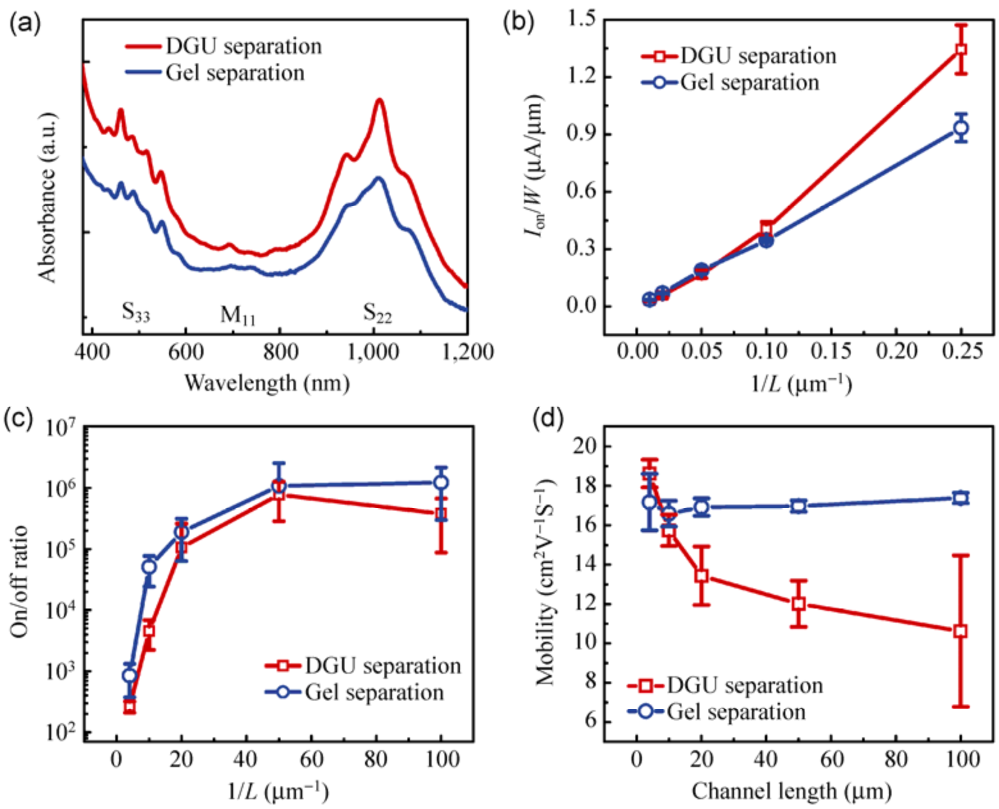

Figure 5 Comparison of key device performance metrics of SN-TFTs using semiconducting arc-discharge nanotubes separated by DGU and gel-based column chromatographic methods. (a) Optical absorption spectra of semiconducting arc-discharge nanotubes separated by DGU (blue) and gel-based column chromatographic (red) methods. (b) Current density (I_{on}/W) versus inverse channel length for TFTs fabricated on semiconducting nanotubes separated by DGU (blue) and gel-based (red) methods. Plots of (c) average on/off ratio (I_{on}/I_{off}) and (d) device mobility (μ_{device}) versus channel length for the same devices measured in (b).

taken at certain gate voltages, one can find that the light intensity of the OLED is modulated by the gate voltage and it can be fully turned on and turned off when V_G are biased at –10 V and 10 V, respectively. Furthermore, current flow through the OLED was also measured by sweeping the V_{DD} while also changing the input voltage V_G as plotted in Fig. 4(b). The figure illustrates that the tested OLED has a threshold voltage of about 3 V and it will be turned on when the controlling transistor is in the "ON" state and the supply voltage is higher than the OLED threshold voltage.

In addition to the comparison of electrical performance between different kinds of gel-based separated semiconducting nanotubes, we are also very interested in the device performance comparison between SN-TFTs using nanotubes separated by gel-based column chromatography and nanotubes separated by other main stream nanotube separation methods, especially the DGU method. To carry out this comparison, we first compared the optical absorption spectra of semiconducting arc-discharge nanotubes separated by DGU (blue curve) and gel-based column chromatographic (red curve) methods, which are shown in Fig. 4(a). Here we chose 99%-separated semiconducting nanotubes purchased from Nanointegris Inc. as the reference DGU-based separated nanotube sample. From this plot, one can find that very similar optical absorption spectra were obtained for DGU-based and gel-based separated nanotubes, which suggests that these two kinds of nanotubes share similar purity as well as diameter distribution. Starting with these two kinds of semiconducting nanotubes, we have fabricated 120 SN-TFTs (60 SN-TFTs having each kind of nanotube) and compared their performance. Figures 5(b)–5(d) summarize the key statistical parameters of the DGU-based and gel-based arc-discharge SN-TFTs. The on-current density and on/off ratio information can be found in Figs. 5(b) and 5(d), which reveal that DGU-based separated SN-TFTs provide slightly higher on-current density but lower on/off ratio than gel-based SN-TFTs. This behaviour may due to the fact that DGU-separated nanotubes have longer average length (~1 μm) than gel-based arc-discharge nanotubes (540 nm) leading to fewer nanotube-to-nanotube junctions and therefore lower sheet resistance, but a higher probability of metallic nanotube pass for DGU-separated nanotubes. Besides on-current and on/off ratio, device mobility is also studied in Fig. 4(d). This figure indicates that gel-based arc-discharge SN-TFTs show slightly higher mobility than DGU-based SN-TFTs when the channel length is longer than 20 μm. Overall, although there are some small differences between gel-based and DGU-based arc-discharge SN-TFTs, these two kinds of devices give similar electrical performance, which suggests that in terms of electrical properties, gel-based separated semiconducting nanotubes are comparable to DGU separated semiconducting nanotubes.

3 Conclusion

We report gel-based column chromatographic nanotube separation of different kinds of nanotubes and their application in macroelectronics, including progress on the detailed analysis of key performance metrics of devices using gel-based arc-discharge, HiPCO, and CoMoCAT semiconducting nanotubes, and direct comparison of the electrical properties of gel-based and DGU-based separated semiconducting nanotubes. We have revealed a trade-off between transistor mobility and on/off ratio, depending on the nanotube diameter. While large-diameter nanotubes (arc-discharge) lead to high device mobility, small-diameter nanotubes (HiPCO and CoMoCAT) can provide high on/off ratios ($> 10^6$) for transistors with comparable dimensions. In addition, based on our analysis, gel-based SN-TFTs have satisfied the requirements of large scale AMOLED high definition displays and can be a promising candidate for the transistors used in next generation displays. Moreover, we have pointed out that due to the trade-off between on-current density and on/off ratio for SN-TFTs, instead of mobility, maximum on-current density for devices with on/off ratio above a certain threshold should be the main parameter to evaluate the electrical performance of carbon nanotube thin-film transistors. Furthermore, we have carried out a comparison between gel-based and DGU-based separated nanotubes, and found that both methods can provide separated nanotubes with similar electrical performance. Our work represents significant advance in gel-based separated nanotube thin-film electronics, and may provide a guide to future research on SN-TFT based macroelectronics.

4 Methods

4.1 Carbon nanotube dispersion

Arc-discharge nanotubes were dispersed in water with the assistant of SC with a concentration of 1 mg/mL, while HiPCO and CoMoCAT nanotubes were dispersed in aqueous solution assisted by 1% SDS (Sigma-Aldrich (99%)) at concentrations of 0.3 mg/mL and 1 mg/mL, respectively. All three kinds of nanotubes were sonicated using a tip-type ultrasonic homogenizer (Sonicator 3000, Misonix) for 2 h at 9 W in a water/ice bath. After sonication, the solution was centrifuged to remove any possible bundles or impurities (20,000 rpm for 3 h at 14 °C). The resulting supernatants were collected as arc-discharge, HiPCO and CoMoCAT single-wall nanotube (SWNT) solutions.

4.2 Nanotube separation by gel-based column chromatography

First, Sephacryl medium (GE Healthcare, Inc.) was filled into a typical column (30 cm in length and 2 cm in diameter). Second, the column was equilibrated by flushing with 1% SDS solution. The nanotube solution was then added to the column. After that 1% SDS solution was used to elute the column, and metallic nanotubes were eluted during this step. Subsequently, for arc-discharge and HiPCO nanotubes, 1% SC solution was added to the column to wash out the remaining semiconducting nanotubes, while 1% SDS + 0.04% SC solution was used to obtain semiconducting CoMoCAT nanotubes.

4.3 Separated nanotube deposition

Aminopropyltriethoxysilane (APTES) was used to functionalize the Si/SiO_2 surface to form an amine-terminated monolayer. This was done by immersing the Si/SiO_2 substrates into diluted APTES solution (1% APTES in isopropanol alcohol (IPA)) for 10 min. The samples were then rinsed with IPA, blown dry thoroughly and then immersed into a solution of separated nanotubes for 30 min, after which uniform nanotube networks were formed on top of the substrates.

4.4 Back-gated SN-TFT fabrication

50 nm SiO_2 was used to act as the back-gate dielectric. The source and drain electrodes were patterned by photo-lithography, and 1 nm Ti and 50 nm Pd were deposited followed by a lift-off process to form the source and drain metal contacts. Finally, since the separated nanotube thin film cover the entire wafer, in order to achieve accurate channel length and width, and to remove any possibility of leakage in the devices, one more step of photo-lithography plus O_2 plasma treatment was used to remove the unwanted nanotubes outside the device channel regions.

Acknowledgements

We acknowledge financial support from Joint King Abdulaziz City for Science and Technology (KACST)/ California Center of Excellence. We thank Dr. Ming Zheng of National Institute of Standards and Technology for valuable discussions.

Electronic Supplementary Material: Raman spectra of arc-discharge, HiPCO, and CoMoCAT semiconducting nanotubes, purity and diameter calculation of gel-based separated nanotubes and plots of off-current versus channel length for three kinds of SN-TFTs are available free of charge via the Internet at http://dx.doi.org/10.1007/s12274-013-0368-9.

References

[1] Iijima, S. Helical microtubules of graphitic carbon. *Nature* **1991**, *354*, 56–58.

[2] Bockrath, M.; Cobden, D. H.; McEuen, P. L.; Chopra, N. G.; Zettl, A.; Thess, A.; Smalley, R. E. Single-electron transport in ropes of carbon nanotubes. *Science* **1997**, *275*, 1922–1925.

[3] Odom, T. W.; Huang, J. L.; Kim, P.; Lieber, C. M. Atomic structure and electronic properties of single-walled carbon nanotubes. *Nature* **1998**, *391*, 62–64.

[4] Wilder, J. W. G.; Venema, L. C.; Rinzler, A. G.; Smalley, R. E.; Dekker, C. Electronic structure of atomically resolved carbon nanotubes. *Nature* **1998**, *391*, 59–62.

[5] Bachtold, A.; Hadley, P.; Nakanishi, T.; Dekker, C. Logic circuits with carbon nanotube transistors. *Science* **2001**, *294*, 1317–1320.

[6] Javey, A.; Guo, J.; Wang, Q.; Lundstrom, M.; Dai, H. J. Ballistic carbon nanotube field-effect transistors. *Nature* **2003**, *424*, 654–657.

[7] Chen, Z. H.; Appenzeller, J.; Lin, Y. M.; Sippel-Oakley, J.; Rinzler, A. G.; Tang, J. Y.; Wind, S. J.; Solomon, P. M.; Avouris, P. An integrated logic circuit assembled on a single carbon nanotube. *Science* **2006**, *311*, 1735.

[8] Liu, X. L.; Lee, C. L.; Zhou, C. W.; Han, J. Carbon nanotube field-effect inverters. *Appl. Phys. Lett.* **2001**, *79*, 3329–3331.

[9] Ryu, K. M.; Badmaev, A.; Wang, C.; Lin, A.; Patil, N.; Gomez, L.; Kumar, A.; Mitra, S.; Wong, H. S. P.; Zhou, C. W. CMOS-analogous wafer-scale nanotube-on-insulator approach for submicrometer devices and integrated circuits using aligned nanotubes. *Nano Lett.* **2009**, *9*, 189–197.

[10] Kang, S. J.; Kocabas, C.; Ozel, T.; Shim, M.; Pimparkar, N.; Alam, M. A.; Rotkin, S. V.; Rogers, J. A. High-performance electronics using dense, perfectly aligned arrays of single-walled carbon nanotubes. *Nat. Nanotechnol.* **2007**, *2*, 230–236.

[11] Ding, L.; Zhang, Z. Y.; Liang, S. B.; Pei, T.; Wang, S.; Li, Y.; Zhou, W. W.; Liu, J.; Peng, L. M. CMOS-based carbon nanotube pass-transistor logic integrated circuits. *Nat. Commun.* **2012**, *3*, 667.

[12] Franklin, A. D.; Chen, Z. H. Length scaling of carbon nanotube transistors. *Nat. Nanotechnol.* **2010**, *5*, 858–862.

[13] Wang, C.; Zhang, J. L.; Ryu, K. M.; Badmaev, A.; De Arco, L. G.; Zhou, C. W. Wafer-scale fabrication of separated carbon nanotube thin-film transistors for display applications. *Nano Lett.* **2009**, *9*, 4285–4291.

[14] Snell, A. J.; Mackenzie, K. D.; Spear, W. E.; LeComber, P. G.; Hughes, A. J. Application of amorphous-silicon field-effect transistors in addressable liquidcrystal display panels. *Appl. Phys.* **1981**, *24*, 357–362.

[15] Forrest, S. R. The path to ubiquitous and low-cost organic electronic appliances on plastic. *Nature* **2004**, *428*, 911–918.

[16] Gelinck, G. H.; Huitema, H. E.; van Veenendaal, E.; Cantatore, E.; Schrijnemakers, L.; van der Putten, J. B. P. H.; Geuns, T. C. T.; Beenhakkers, M.; Giesbers, J. B.; Huisman, B. H. et al. Flexible active-matrix displays and shift registers based on solution-processed organic transistors. *Nat. Mater.* **2004**, *3*, 106–110.

[17] Klauk, H.; Halik, M.; Zschieschang, U.; Eder, F.; Rohde, D.; Schmid, G.; Dehm, C. Flexible organic complementary circuits. *IEEE Trans. Electron Devices* **2005**, *52*, 618–622.

[18] Uchikoga, S. Low-temperature polycrystalline silicon thin-film transistor technologies for system-on-glass displays. *MRS Bull.* **2002**, *27*, 881–886.

[19] Chang, C. P.; Wu, Y. S. Improved electrical performance of MILC poly-Si TFTs using CF4 plasma by etching surface of channel. *IEEE Electron Device Lett.* **2009**, *30*, 130–132.

[20] Nomura, K.; Ohta, H.; Ueda, K.; Kamiya, T.; Hirano, M.; Hosono, H. Thin-film transistor fabricated in single-crystalline transparent oxide semiconductor. *Science* **2003**, *300*, 1269–1272.

[21] Nomura, K.; Ohta, H.; Takagi, A.; Kamiya, T.; Hirano, M.; Hosono, H. Room-temperature fabrication of transparent flexible thin-film transistors using amorphous oxide semiconductors. *Nature* **2004**, *432*, 488–492.

[22] Arnold, M. S.; Stupp, S. I.; Hersam, M. C. Enrichment of single-walled carbon nanotubes by diameter in density gradients. *Nano Lett.* **2005**, *5*, 713–718.

[23] Arnold, M. S.; Green, A. A.; Hulvat, J. F.; Stupp, S. I.; Hersam, M. C. Sorting carbon nanotubes by electronic structure using density differentiation. *Nat. Nanotechnol.* **2006**, *1*, 60–65.

[24] Engel, M.; Small, J. P.; Steiner, M.; Freitag, M.; Green, A. A.; Hersam, M. C.; Avouris, P. Thin film nanotube transistors based on self-assembled, aligned, semiconducting carbon nanotube arrays. *ACS Nano* **2008**, *2*, 2445–2452.

[25] Sangwan, V. K.; Ortiz, R. P.; Alaboson, J. M. P.; Emery, J. D.; Bedzyk, M. J.; Lauhon, L. J.; Marks, T. J.; Hersam, M. C. Fundamental performance limits of carbon nanotube thin-film transistors achieved using hybrid molecular dielectrics. *ACS Nano* **2012**, *6*, 7480–7488.

[26] Wang, C.; Zhang, J. L.; Zhou, C. W. Macroelectronic integrated circuits using high-performance separated carbon nanotube thin-film transistors. *ACS Nano* **2010**, *4*, 7123–7132.

[27] Zhang, J. L.; Wang, C.; Fu, Y.; He, Y. C.; Zhou, C. W. Air-stable conversion of separated carbon nanotube thin-film transistors from p-type to n-type using atomic layer deposition of high-kappa oxide and its application in CMOS logic circuits. *ACS Nano* **2011**, *5*, 3284–3292.

[28] Zhang, J. L.; Wang, C.; Zhou, C. W. Rigid/flexible transparent electronics based on separated carbon nanotube thin-film transistors and their application in display electronics. *ACS Nano* **2012**, *6*, 7412–7419.

[29] Zhang, J. L.; Fu, Y.; Wang, C.; Chen, P. C.; Liu, Z. W.; Wei, W.; Wu, C.; Thompson, M. E.; Zhou, C. W. Separated carbon nanotube macroelectronics for active matrix organic light-emitting diode displays. *Nano Lett.* **2011**, *11*, 4852–4858.

[30] Tanaka, T.; Jin, H. H.; Miyata, Y.; Fujii, S.; Suga, H.; Naitoh, Y.; Minari, T.; Miyadera, T.; Tsukagoshi, K.; Kataura, H. Simple and scalable gel-based separation of metallic and semiconducting carbon nanotubes. *Nano Lett.* **2009**, *9*, 1497–1500.

[31] Moshammer, K.; Hennrich, F.; Kappes, M. M. Selective suspension in aqueous sodium dodecyl sulfate according to electronic structure type allows simple separation of metallic from semiconducting single-walled carbon nanotubes. *Nano Res.* **2009**, *2*, 599–606.

[32] Liu, H. P.; Nishide, D.; Tanaka, T.; Kataura, H. Large-scale single-chirality separation of single-wall carbon nanotubes by simple gel chromatography. *Nat. Commun.* **2011**, *2*, 309.

[33] Gui, H.; Li, H. B.; Tan, F. R.; Jin, H. H.; Zhang, J.; Li, Q. W. Binary gradient elution of semiconducting single-walled carbon nanotubes by gel chromatography for their separation according to chirality. *Carbon* **2012**, *50*, 332–335.

[34] Miyata, Y.; Shiozawa, K.; Asada, Y.; Ohno, Y.; Kitaura, R.; Mizutani, T.; Shinohara, H. Length-sorted semiconducting carbon nanotubes for high-mobility thin film transistors. *Nano Res.* **2011**, *4*, 963–970.

[35] Miyata, Y.; Yanagi, K.; Maniwa, Y.; Kataura, H. Optical evaluation of the metal-to-semiconductor ratio of single-wall carbon nanotubes. *J. Phys. Chem. C* **2008**, *112*, 13187–13191.

[36] Nirmalraj, P. N.; Lyons, P. E.; De, S.; Coleman, J. N.; Boland, J. J. Electrical connectivity in single-walled carbon nanotube networks. *Nano Lett.* **2009**, *9*, 3890–3895.

[37] Asada, Y.; Nihey, F.; Ohmori, S.; Shinohara, H.; Saito, T. Diameter-dependent performance of single-walled carbon nanotube thin-film transistors. *Adv. Mater.* **2011**, *23*, 4631–4635.

[38] Pike, G. E.; Seager, C. H. Percolation and conductivity: A computer study. I. *Phys. Rev. B* **1974**, *10*, 1421–1434.

[39] Kwon, O. K. TFT mobility requirement for AMOLED HDTVs. *Thin film transistor technologies (TFTT VII): proceedings of the international symposium* **2004**, 146.

[40] Gu, G.; Forrest, S. R. Design of flat-panel displays based on organic light-emitting devices. *IEEE J. Sel. Top. Quantum Electron.* **1998**, *4*, 83–99.

[41] Kang, S. J.; Kocabas, C.; Ozel, T.; Shim, M.; Pimparkar, N.; Alam, M. A.; Rotkin, S. V.; Rogers, J. A. High-performance electronics using dense, perfectly aligned arrays of single-walled carbon nanotubes. *Nat. Nanotechnol*. **2007**, *2*, 230–236.

[42] Cao, Q.; Xia, M. G.; Kocabas, C.; Shim, M.; Rogers, J. A.; Rotkin, S. V. Gate capacitance coupling of singled-walled carbon nanotube thin-film transistors. *Appl. Phys. Lett*. **2007**, *90*, 023516.

[43] Rosenblatt, S.; Yaish, Y.; Park, J.; Gore, J.; Sazonova, V.; McEuen, P. L. High performance electrolyte gated carbon nanotube transistors. *Nano Lett*. **2002**, *2*, 869–872.